Electronic Supplementary Material (ESI) for Journal of Materials Chemistry C.
This journal is © The Royal Society of Chemistry 2019

Supporting Information – Predicting the yield of ion pair formation in molecular electrical doping: redox-potentials *versus* ionization energy / electron affinity

Berthold Wegner[1,2], Lutz Grubert[3], Dennis Chercka[4], Andreas Opitz[2], Adriana Röttger[2], Yadong Zhang[5], Stephen Barlow[5], Seth R. Marder[5], Stefan Hecht[3], Klaus Müllen[4], and Norbert Koch[1,2]*

[1] Helmholtz-Zentrum Berlin für Materialien und Energie GmbH, Albert-Einstein-Str. 15, D-12489 Berlin, Germany

[2] Institut für Physik & IRIS Adlershof, Humboldt-Universität zu Berlin, Brook-Taylor-Str. 6, D-12489 Berlin, Germany

[3] Institut für Chemie, Humboldt-Universität zu Berlin, Brook-Taylor-Straße 2, D-12489 Berlin, Germany

[4] Max-Planck-Institut für Polymerforschung, Ackermannweg 10, D-55128 Mainz, Germany

[5] School of Chemistry and Biochemistry and Center for Organic Photonics and Electronics (COPE), Georgia Institute of Technology GA, Atlanta 30332-0400, USA

Contents

1. Additional information on the preparation of PFP:$CoCp_2$ mixed solutions and thin films

Since the solubility of PFP in the used solvent (DCM) is poor and not even concentrations of 0.1 mM could be achieved without precipitants of non-dissolved PFP being present, saturated PFP solutions (< 0.1 mM) were used and mixed with (excess) $CoCp_2$. This approach was used to show the general feasibility of IPA formation between PFP and $CoCp_2$ in solution, since it was found that the PFP anions are not stable in solution (the peak associated with ionized PFP at 0.65 eV measured on a PFP solution with excess $CoCp_2$ vanished during the course of an hour, while the peak of neutral PFP re-appeared in part). This is not surprising, since the anions of PFP can be expected to be air- and moisture sensitive. According to the specification sheet of the commercially purchased, anhydrous DCM (Sigma Aldrich, anhydrous, ≥99.8%), the used DCM still contains up to 10 ppm of water. However, 10 ppm water correspond to a molar concentration of 0.5 mM (by using the general convention of 1 ppm ≈ 1 mg l^{-1}). Due to the low solubility and thus the used low concentration of PFP (< 0.1 mM), the amount of PFP (thus PFP anions) and water in the DCM solution can be assumed to be in the same order of magnitude, explaining the instability of the PFP anions in this setup. For this reason, using lower concentrations with fully dissolved PFP (in the order of 10^{-5} M) would not have been beneficially to determine the IPA formation yield.

Due to the low solubility of PFP, it was not possible to deposit useable thin films from solution. Furthermore, the vacuum deposition of $CoCp_2$ is also rather complicated – due to its high vapor pressure, $CoCp_2$ has to be introduced to the vacuum system from an ampoule via a leak valve[1] – and thus depositing mixed thin films in a molar 1:1 ratio cannot be achieved easily. For this reason, mixed films of PFP:$CoCp_2$ were fabricated by dipping a vacuum deposited PFP thin film (ca. 50 nm) into a 2 mM solution of $CoCp_2$ in DCM, and by sequentially spin-coating the 2mM $CoCp_2$ solution onto a PFP film. Sequential spin-coating was performed by dropping 100 µl of the $CoCp_2$ solution onto the spinning PFP thin film (6000 rpm). In both cases, incorporation of $CoCp_2$ into the thin film is sought to occur due to swelling of the PFP thin film caused by the DCM solution.

2. Cyclic voltammetry data for the materials of set I

Figure S1 shows the cyclic voltammograms for the materials of set I in solution (DCM). The obtained half-wave potentials are summarized in Table S1.

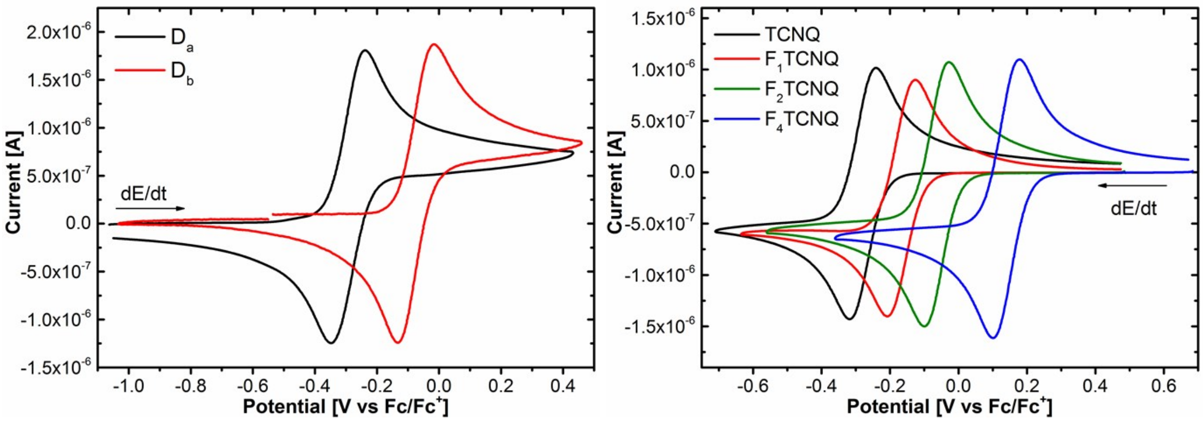

Figure S1. CV measurements for the used donors D_x (**left**) and the acceptors F_xTCNQ (**right**). The scanning direction is indicated with an arrow marked by dE/dt.

Table S1. Summary of the obtained oxidation / reduction half-wave potentials $E_{1/2}^{ox}$ / $E_{1/2}^{red}$ of the used donors / acceptors, respectively.

	$E_{1/2}^{ox}$ [mV vs. Fc/Fc$^+$]		**$E_{1/2}^{red}$ [mV vs. Fc/Fc$^+$]**
D_a	-266	**TCNQ**	-290
D_b	-44	**F_1TCNQ**	-179
		F_2TCNQ	-71
		F_4TCNQ	130

3. Changes in the UV-Vis-spectra of the donors D_x during cyclic voltammetry

Figure S2 summarizes the data from spectro-electrochemistry for the molecules D_a and D_b. The spectra at the beginning of the oxidation are in both cases comparable to the spectra obtained by doping the donors with FeCl3 in solution (see Figure S5 for comparison). The changes in the absorption spectra at a later stage of oxidation are, however, not yet understood and need further investigation. The oxidation process is fully reversible, as the absorption spectrum after voltage cycling is identical with the spectrum before (not displayed here).

Spectro-electrochemistry was performed in a SEC-C thin layer quartz glass spectro-electrochemical cell (0.5 mm optical path length, working electrode: platinium mesh, counter electrode: platinum wire, reference electrode: non aqueous reference electrode Ag/Ag^+ with 0.01 M $AgNO_3$ and 0.1 M Bu_4NPF_6 in acetonitrile) from ALS Co. Ltd (Tokyo, Japan) using the Potentiostat PGSTAT 128N (Deutsche Metrohm GmbH & Co. KG, Filderstadt, Germany) and the software NOVA 2.10. Absorption measurements were performed using the spectrometers AvaSpec-2048x14 with AvaLigth-DH-S-BAL and the software AvaSoft 7.7.2 (both Avantes, Apeldoorn, Netherlands).

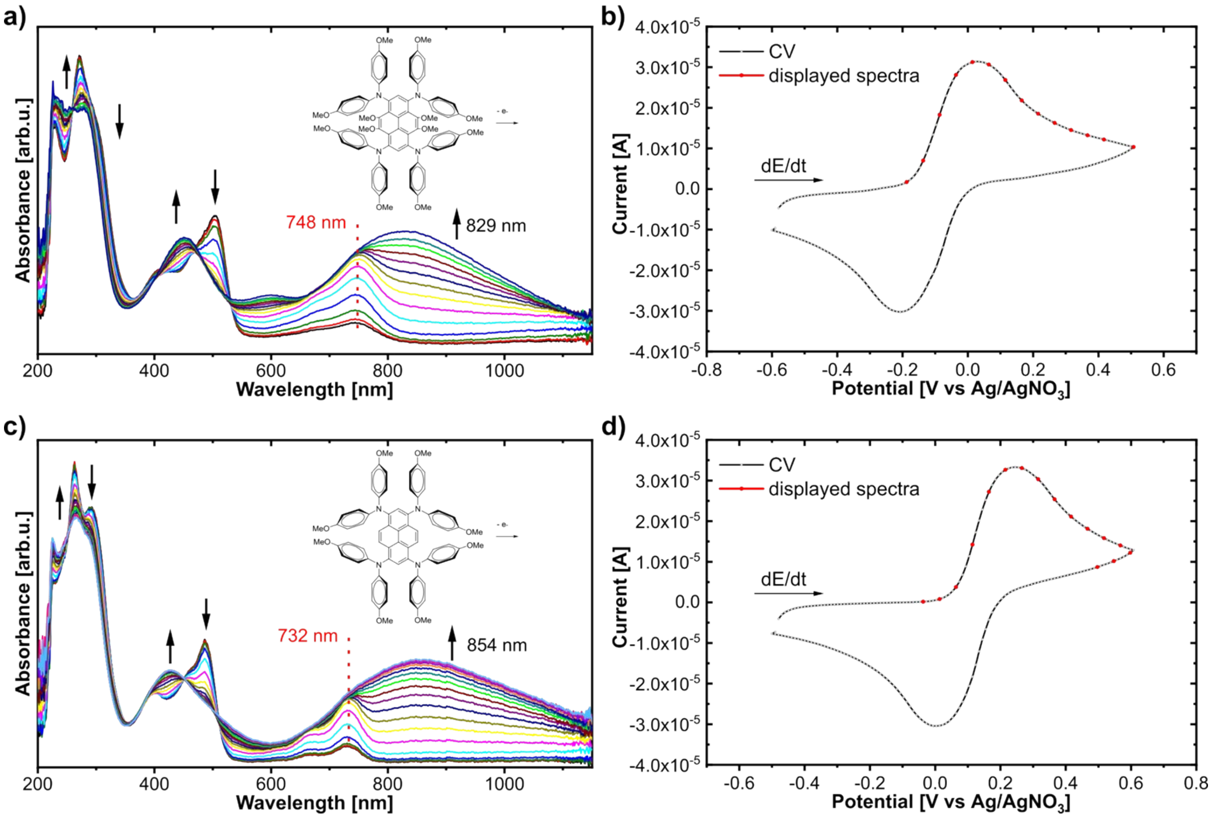

Figure S2. a) Changes in the UV-Vis-spectra of D_a during cyclic voltammetry. **b)** 2D-Plot of D_a (c = 5.0 10^{-4} mol/l in 0.1 M Bu_4NPF_6 DCM): Buildup of the radical cation $D_a^{\cdot+}$ Range of -0.19 → 0.50 V [$Ag/AgNO_3$], scan rate dE/dt 10 mV/s, Range of -0.60 → 0.50 → -0.60 V [$Ag/AgNO_3$], quartz cuvette, d = 0.5 mm. **c)** Changes in the UV-Vis-spectra of D_b during cyclic voltammetry. **d)** 2D-Plot of D_b (c = 3.58 10^{-4} mol/l in 0.1 M Bu_4NPF_6 DCM): Buildup of the radical cation $D_b^{\cdot+}$ Range of -0.04 → 0.60 → 0.50 V [$Ag/AgNO_3$], scan rate dE/dt 10 mV/s, Range of -0.50 → 0.60 → -0.50 V [$Ag/AgNO_3$], quartz cuvette, d = 0.5 mm.

4. Ultraviolet photoelectron spectra of the donors D_x

Figure S3 shows the spectra of the UPS measurements on thin films of the donors D_x. Samples for UPS measurements were prepared via spin-coating (20 / 40 rps) of the respective DCM solutions on solvent cleaned and UV-ozone treated indium tin oxide substrates under inert atmosphere. Spin-coating with 40 and 20 rps yielded thin films with a thickness of around 5 (sample 1) and 8 nm (sample 2), respectively, as determined by scanning force microscopy on reference samples. After preparation, the samples were transferred to the vacuum system without exposure to air. From the obtained results summarized in Table S2 the ionization energy (IE) of D_a and D_b was determined to be 4.67 eV and 4.90 eV, respectively.

Table S2. Summary of obtained UPS results.

		Φ [eV]	**HOMO [eV]**	**IE [eV]**
D_a	Sample 1	4.18	0.49	4.67
	Sample 2	4.15	0.52	4.67
D_b	Sample 1	4.40	0.51	4.91
	Sample 2	4.31	0.58	4.89

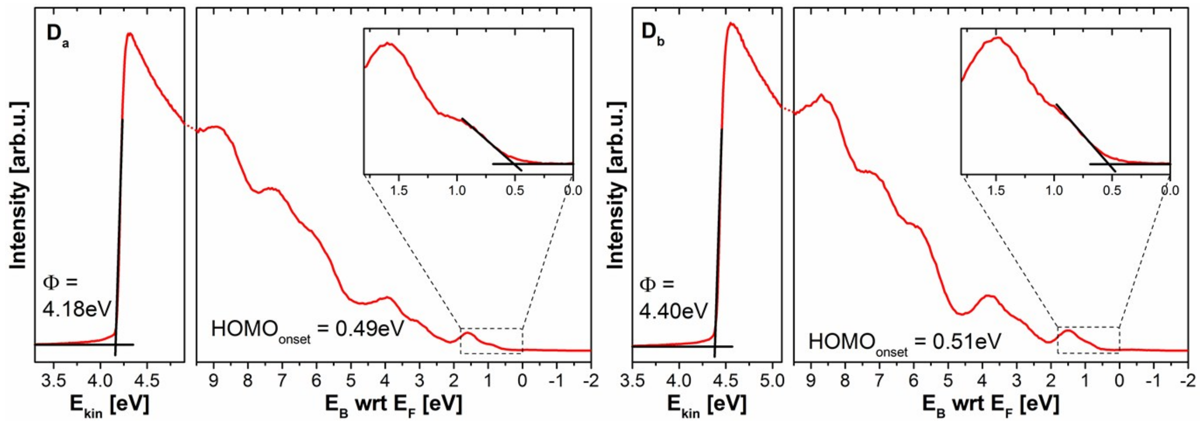

Figure S3. UPS Spectra of the donors D_a (**left**) and D_b (**right**). The left panel shows the SECO with respect to the kinetic energy E_{kin} from which the work function Φ of the samples was determined. The right panel shows the valence structure of the molecules with respect to the binding energy E_b, where 0 eV corresponds to the Fermi level E_F. The inlet in the right panel shows the onset of the HOMO level magnified for better visibility.

5. Optical spectra of the F_xTCNQs in solution

Figure S4 shows the optical spectra of the F_xTCNQ acceptors in solution. From the spectra in solution it can be seen that none of the acceptors is ionized in DCM and the neutral molecules do not absorb in the spectral region up to around 2.5 eV. Reference spectra of the ionized F_xTCNQ can be found in the supporting information of ref. (2).

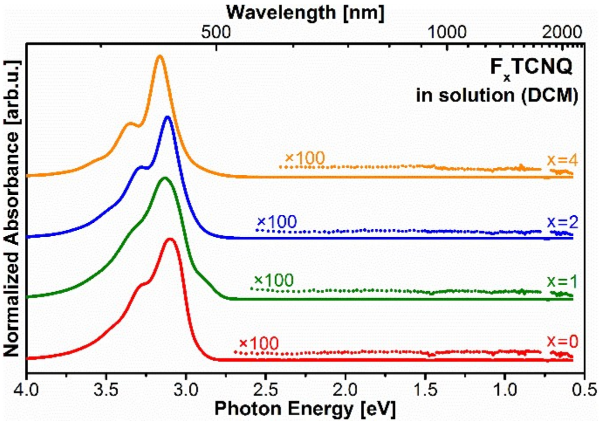

Figure S4. Optical reference spectra of F_xTCNQ in solution (DCM) with 100× magnified absorbance in the region up to around 2.5 eV.

6. Identification of ionic species

6.1 Set I

To identify the emerging peaks in the mixed solutions and thin films of material set I, reference spectra were recorded of the ionized donors and acceptors. For this reason, iron(III) chloride ($FeCl_3$) and potassium iodide (KI) were added in increasing amounts to the donor and acceptor solutions, respectively, and the evolution of the ionized peaks was followed by optical absorption spectroscopy.

Figure S5 shows the optical spectra of the systems D_x:F_4TCNQ (both in solution and as thin films) in comparison to the optical spectra of the ionized D_x / F_4TCNQ in solution. Since the peaks related to the F_xTCNQ radical anion are very similar (compare ref. 2), the systems with F_4TCNQ are shown here as representatives for all systems. From Figure S5 it can be seen that the spectra of the mixed solutions and thin films are very similar. The features of the spectra of the mixed thin films are slightly red-shifted and broadened in comparison to the spectra of the mixed solutions (as would be expected). By comparing the spectra of the mixed systems with the reference spectra of the ionized donors / acceptors, the feature at 1.0 eV can be associated with the cation of the donors, the one at 1.4 eV with the anion of the acceptors and the features at 1.6 to 1.8 eV can be identified as a superposition of both cation and anion features.

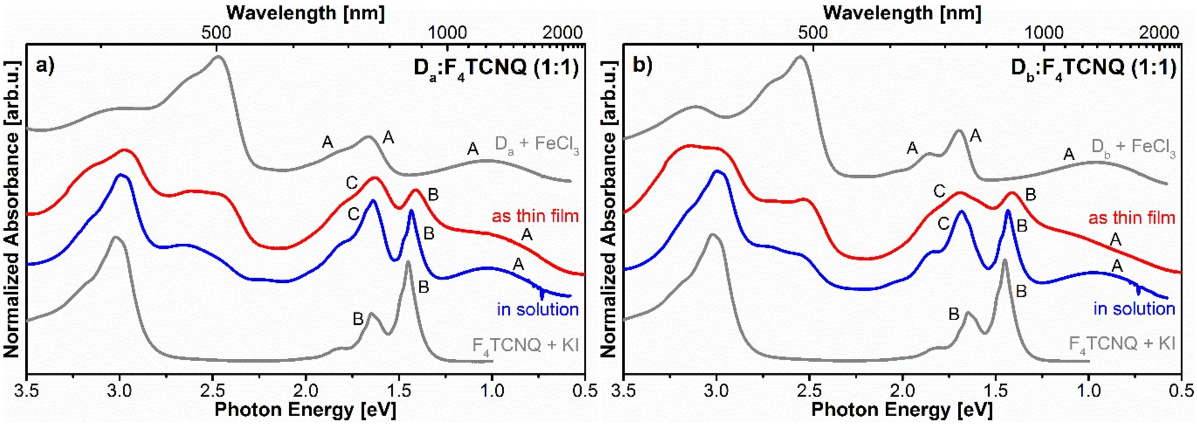

Figure S5. Comparison of the optical spectra of **a)** D_a:F_4TCNQ and **b)** D_b:F_4TCNQ of solutions and thin films with reference spectra and attribution of absorption features belonging to ionic species. By comparison with the reference spectra the new emerging peaks in the range of 0.5 to 2.0 eV can be attributed to the cation features of D_x (A), the anion features of F_4TCNQ (B) and a superposition of both (C).

6.2 Set II

Figure S6a shows the optical spectra of 6T and DH6T in solution (DCM). Due to poor solubility of both compounds in DCM, saturated solutions were used. $FeCl_3$ was added to both solutions to generate cations of the oligothiophenes. Both spectra show similar new features in the region up to 2.0 eV. The position of these new features are at 0.78 eV, 0.94 eV, 1.53 eV and 1.75 eV for DH6T and 0.85 eV, 1.01 eV, 1.59 eV and 1.81 eV for 6T, while the positions of the main neutral 6T and DH6T features are at 2.85 eV and 2.79 eV, respectively. These values are comparable to previously reported values for the cation of 6T.[3] Figure S6b shows the optical spectra of $Mo(tfd)_3$ in solution ($CHCl_3$). By titration with a lithium iodide (LiI) solution, the anions of $Mo(tfd)_3$ can be generated. Here, with increasing LiI concentration the feature of the neutral molecule at 2.13 eV is decreasing, while two new features at 1.89 eV and 1.34 eV are increasing. The spectra are in good agreement with previously reported spectra for the reduction of $Mo(tfd)_3$ with ferrocene.[4]

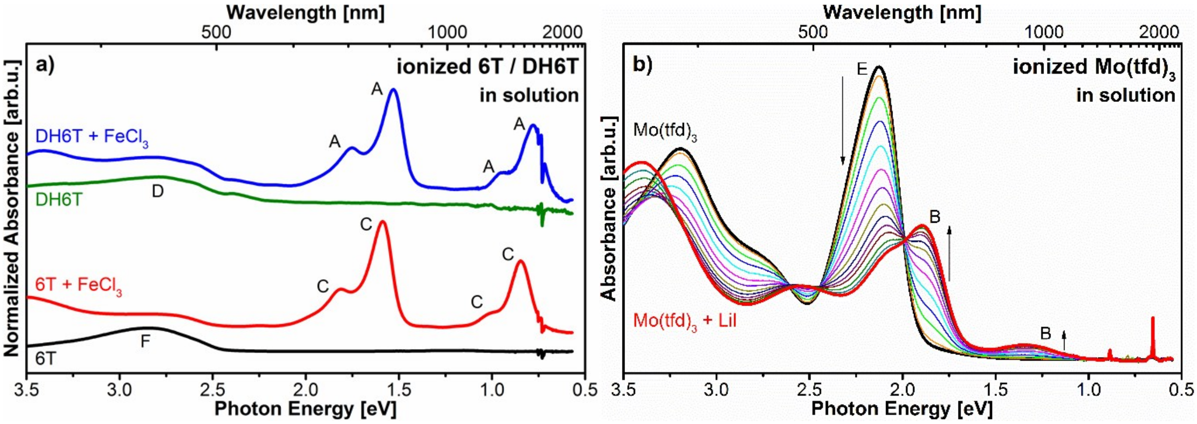

Figure S6. Optical spectra of **a)** ionized 6T / DH6T and **b)** ionized Mo(tfd)$_3$ in solution. The features of ionized DH6T, Mo(tfd)$_3$ and 6T are marked with A, B and C, respectively, while the neutral features of these compounds are marked with D, E and F, respectively.

In literature, the molar absorptivity for 6T is reported to be 5.0×10^4 M^{-1}cm^{-1} (at 436 nm in THF)[5] and 6.0×10^4 M^{-1}cm^{-1} (at 432 nm in DCM)[6] and for its cation 6T$^+$ to be 4.3×10^4 M^{-1}cm^{-1} (at 780 nm in DCM)[7], while for DH6T it is reported to be 5.3×10^4 M^{-1}cm^{-1} (at 440 nm in THF)[5]. Since the molar absorptivity for 6T and DH6T in THF is roughly the same, it is assumed here that also the molar absorptivities for the cations are roughly the same. Based on Figure S6a and the reported molar absorptivity of 6T$^+$ at 780nm (1.59 eV), the molar absorptivity of the cation feature at 0.84 eV is calculated to be around 2.8×10^4 M^{-1}cm^{-1}. Using these values of molar absorptivities and the intensity ratios of the features of ionized and neutral DH6T/6T species from Figure 3 (0.6% and 2.2%, respectively), the ratio between ionized and neutral species is estimated to be in the order of 1% for DH6T:Mo(tfd)$_3$ in solution and 4% for 6T:Mo(tfd)$_3$ in a thin film.

6.3 Set III

Reference spectra for the CoCp$_2$ cation can be found in literature with its lowest transition lying at around 3 eV.[8,9] For PFP it was not possible to generate anions by reduction with KI or LiI, nor cations by oxidation with FeCl$_3$. Also spectroelectrochemical measurements did not yield reasonable results. For this reason, the appearing features in the spectral region of 0.5 to 2.0 eV for PFP:CoCp$_2$ thin films and solutions (Figure 4) will be assigned to belong to the PFP anions by comparison with the optical spectra of PEN cations. The main reasoning here is the similarity of the optical spectra of PEN and PFP, and that usually the optical features of anions and cations are very similar.[10] PEN cations were generated by titration of a FeCl$_3$ solution to a saturated PEN solution (DCM), the optical spectra of which are displayed in Figure S6c.

Figures S7 a & b show the optical spectra of pure PEN and PFP in thin films and solutions, respectively. As can be seen, the optical features are very similar, with the main difference of the PFP spectra being red-shifted to the PEN spectra by 110 meV for the thin films and 155 meV for the solutions. Especially in solution the features of the first optical transitions show the same structure (only the intensity of the transitions being different) and are separated by ca. 170 meV. The features of the saturated pure PFP and PEN solutions at 1.7 eV and 1.8 eV can be assigned to non-dissolved particles, since the respective thin films show absorption features at these energies and they are not present in literature specta.[11] Figure S6c shows the optical spectra of PEN cations. Here, upon titration of FeCl$_3$ new features are emerging in spectral range of 0.5 to 2.0 eV (labeled A) and the positions of the first four strong transitions are lying at 1.07 eV, 1.27 eV, 1.44 eV, and 1.61 eV (thus all separated by 170 to 200 meV).

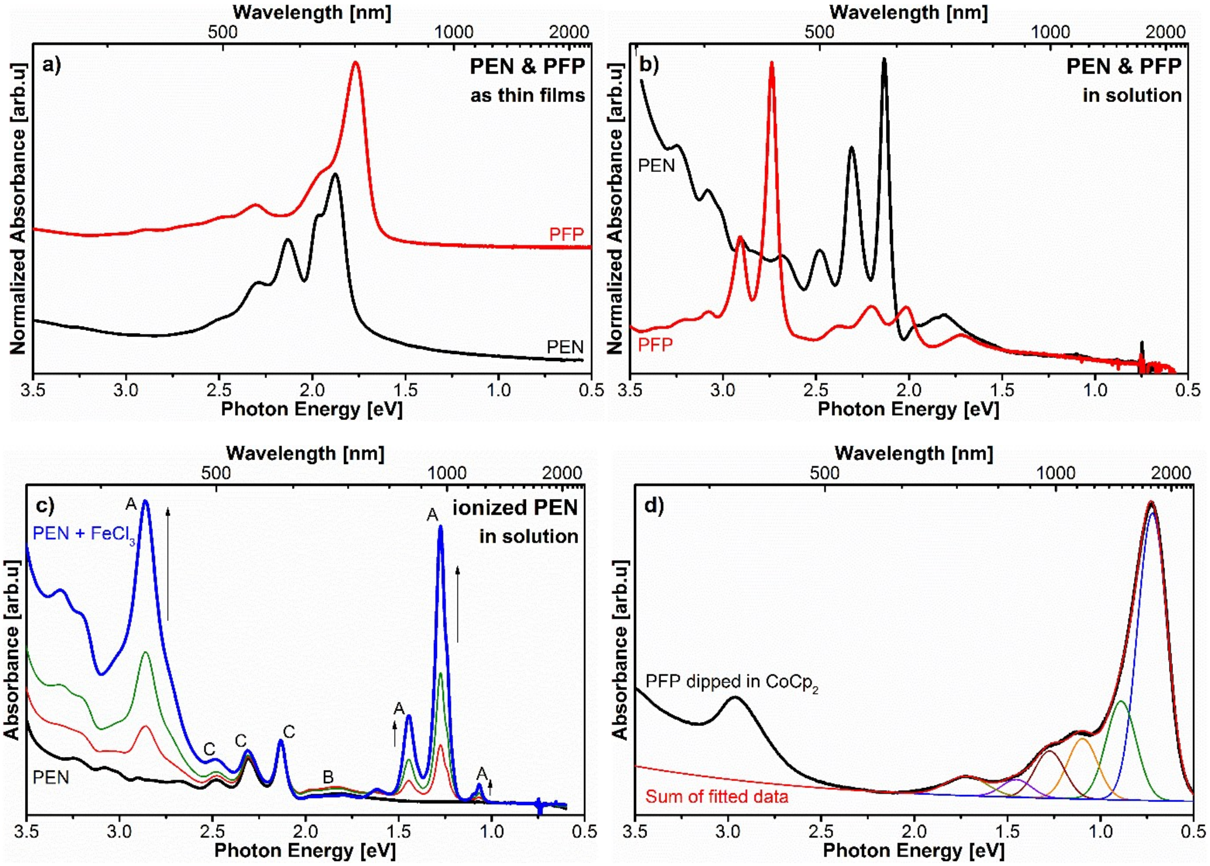

Figure S7. Optical spectra of **a)** pentacene (PEN) and PFP as thin films and **b)** in solution. Both spectra show similar optical features, especially in solution, where just the intensity of the features is different. The maximum of the first optical transition of the PFP thin film is red shifted compared to PEN by 110 meV and in solution by 155 meV. The features at 1.7 eV and 1.8 eV for PFP and PEN in solution stem from non-dissolved particles. **c)** Optical spectra of PEN cations generated by titration with a $FeCl_3$ solution. The features can be assigned to PEN cations (A), non-dissolved PEN (B) and neutral PEN (C). **d)** Spectra of PFP film dipped in a $CoCp_2$ solution. The features in the spectral region of 0.5 to 2.0 eV were fitted with Gaussian peaks to reveal the optical structure of ionized PFP.

The neutral features (C) at 2.13 eV and 2.31 eV are not vanishing upon $FeCl_3$ titration, since due to poor solubility a saturated PEN solution was used with non-dissolved PEN still being present. Thus, when PEN is ionized (ionized PEN is more soluble), some of the non-dissolved PEN particles will dissolve, basically keeping the neutral PEN concentration constant. To compare the structure of the newly appearing features in the thin films of PFP:$CoCp_2$, the features in the spectral region of 0.5 to 2.0 eV of the PFP thin film dipped into a $CoCp_2$ solution were fitted by using Gaussian peaks and a background (as described in the experimental section). Figure S7d shows the fitted spectrum which reveals the first four strong transitions to lie at 0.72 eV, 0.89 eV, 1.10 eV, and 1.27 eV. Again all features are separated by 170 to 200 meV, similar to the structure of PEN cations with of course the intensity of the transitions being different. In general for PEN and PFP, the energetically lowest transition is strongest in the thin films. When we assume that the red shift of PEN to PFP and from solution to thin films is the same for the ionized species, we can estimated the position of the first transition for ionized PFP species. The red shift from solution to thin film of the first optical transition for PEN is 270 meV, while the red shift of PEN to PFP thin film is 110 meV. Applying these shifts to the energetically lowest transition of PEN cations at 1.07 eV, the estimated position for the first transition of ionized PFP is 0.69 eV. This value is very close to the position of the energetically lowest transition of the PFP:$CoCp_2$ thin film (Figure S7d) at 0.72 eV. Therefore, by comparison of the structure of the optical features and the shifts in PEN and

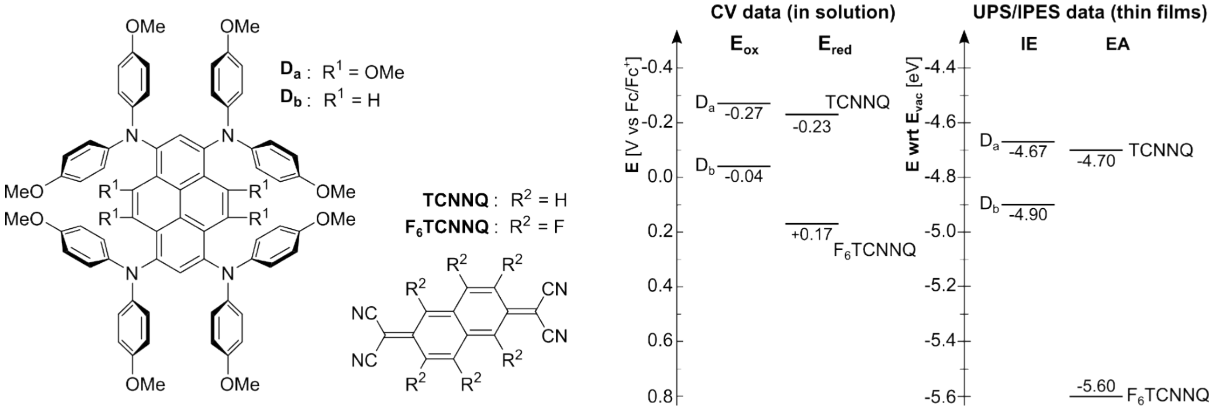

Figure S8. Chemical structures (left) and energy level diagrams deduced from CV and UPS/IPES data (right) of the donors D_x and the acceptors 11,11,12,12-tetracyanonaphtho-2,6-quinodimethane (TCNNQ) and 1,3,4,5,7,8-hexafluoro-tetracyanonaphtho-2,6-quinodimethane (F_6TCNNQ). IPES data of the F_xTCNNQ were taken from literature.[12,13]

PFP thin films and solutions, we can safely assign the newly appearing features in the optical spectra of PEN:$CoCp_2$ displayed in Figure 4 to belong to ionized PFP.

7. Supporting measurements employing the acceptors F_xTCNNQ

To further support the results of set I, experiments with additional acceptors – 11,11,12,12-tetracyanonaphtho-2,6-quinodimethane (TCNNQ) and 1,3,4,5,7,8-hexafluoro-tetracyanonaphtho-2,6-quino-dimethane (F_6TCNNQ) – were conducted. These two acceptors are similar in their structures as well as their energy levels to the F_xTCNQs (see Figure S9) and, thus, they represent a good extension to set I.

In the case of F_xTCNNQ, the CV and UPS/IPES data provide the same predictions about the ionization yield. While charge transfer from both donors should proceed with a high yield to F_6TCNNQ, charge transfer to TCNNQ should only proceed with a high yield from D_a and with a low yield from D_b. The optical spectra of solutions shown in Figure S9 a & b prove this prediction to be correct. Here, the ionization yield of both donors with F_6TCNNQ is around 100%. For TCNNQ, the ionization yield was found to be around 50% in the case of D_a and less than 1% in the case of D_b. The via thermodynamic consideration estimated charge transfer probabilities (see section 7) are again in reasonably good quantitative agreement with the experimental results as shown in Table S3.

Table S3. Charge transfer probability (P_{theo}) as function of the difference in electrochemical potential (ΔE) in comparison with measured yield of ionized molecules in solution (P_{exp}).

	ΔE [mV]		**P_{theo} [%]**		**P_{exp} [%]**	
	D_a	**D_b**	**D_a**	**D_b**	**D_a**	**D_b**
TCNNQ	40	-190	69	2	50	0.4
F_6TCNN	440	210	100	99	100	100

When turning from solutions to solid thin films (Figure S9 c & d), the same effect which occurred for F_xTCNQ is observed. Namely, in the case of D_a:TCNNQ, a higher amount of molecules (from the spectrum estimated to be >80%) is found to have undergone charge transfer in the thin film than in solution. This is ascribed to the same reasons as described in the main text. In the case of F_6TCNNQ, charge transfer is again found to proceed with a yield in the range of 100%, while for D_b:TCNNQ, the ionization yield is estimated to be <5%. Due to the fact, that both CV and UPS/IPES data provide the same predictions about the ionization yields, the presented results cannot be used to gain further insights into which experimentally determined energy level values are more reliable to predict ion pair formation. Nonetheless, the presented data of the F_xTCNNQs are consistent with the data of the F_xTCNQs and thus, a useful extension to set I.

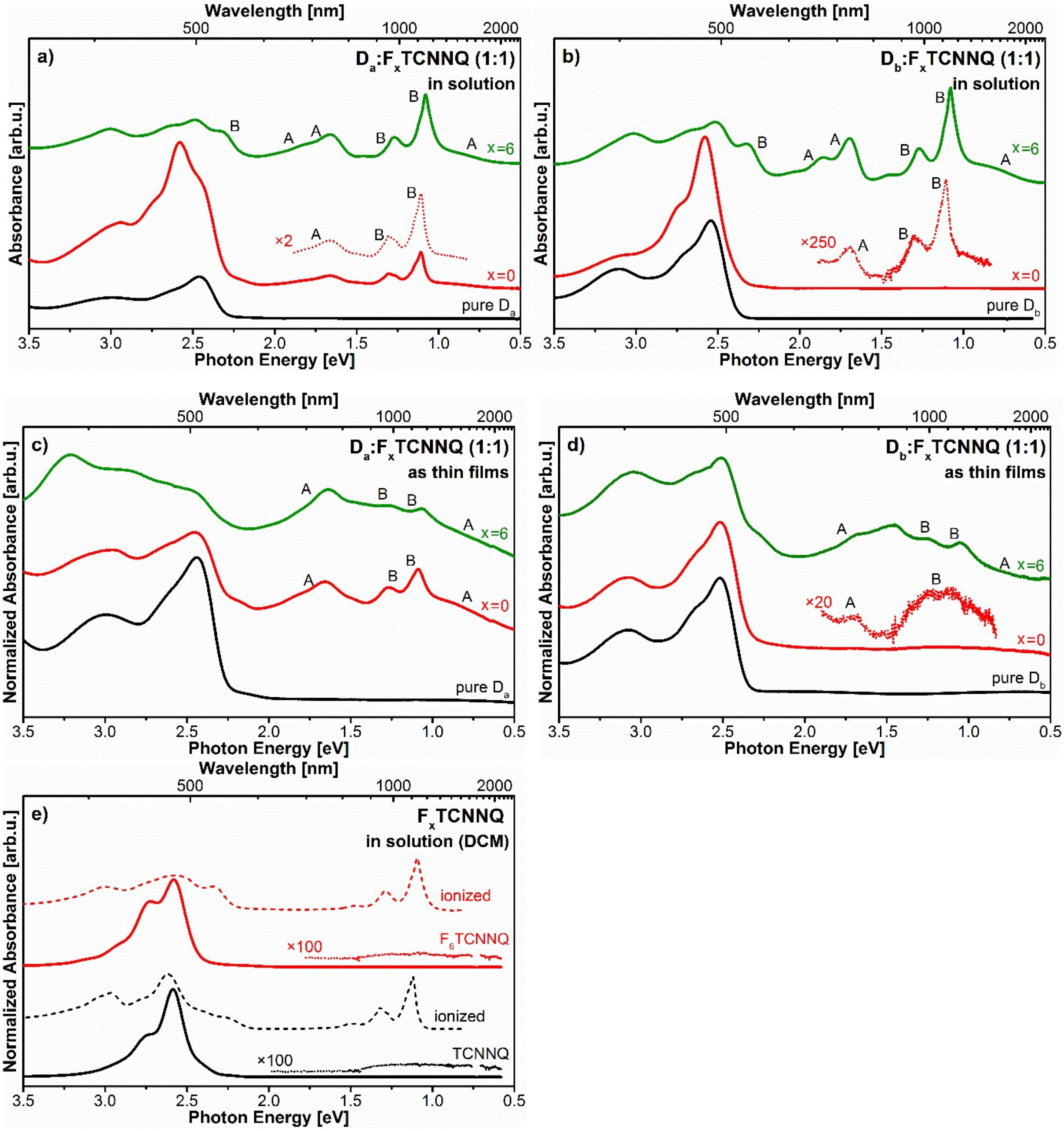

Figure S9. Optical spectra of **a)** D_a:F_xTCNNQ in solution, **b)** D_b:F_xTCNNQ in solution, **c)** D_a:F_xTCNNQ in thin films, and **d)** D_b:F_xTCNNQ in thin films. By comparison with reference spectra, the new emerging peaks in the range of 0.5 to 2.0 eV can be attributed to the cation features of D_x (A) and the anion features of F_xTCNNQ (B). The solution spectra show that only in the systems with F_6TCNNQ nearly all the molecules ionize, while for D_a:TCNNQ 50% and for D_b:TCNNQ only 0.4% of the molecules undergo charge transfer. In thin films, change transfer proceeds efficiently with a high yield in all systems except D_b:TCNNQ, where only a small percentage of molecules is ionized (<5%). **e)** Optical reference spectra of F_xTCNNQ in solution (DCM) with 100× magnified absorbance in the region up to around 2.5 eV. Ionized F_xTCNNQ were created by adding lithium iodide (LiI) to the respective solutions, the spectra of which are shown as dashed lines.

8. Calculation of charge transfer probability

The probability for (or the percentage of molecules which undergoes) charge transfer in the donor-acceptor (D-A) systems in solution for a given difference in electrochemical potential was estimated using basic thermodynamic considerations for the reaction $D + A \rightleftharpoons D^{+} + A^{-}$ in equilibrium. Following Nernst's equation,[14] we get

$$\ln K = \frac{z_e F \Delta E}{RT} \quad \textit{with} \quad \Delta E = E_{1/2}^{red} - E_{1/2}^{ox}, \tag{1}$$

where $\ln K$ is the natural logarithm of the equilibrium constant, z_e the number of moles of transferred electrons, F Faraday's constant, R the gas constant, T the absolute temperature (here 20° C – 293.15 K), $E_{1/2}^{red}$ the half-wave reduction potential of the acceptors and $E_{1/2}^{ox}$ the half-wave oxidation potential of the donors. The equilibrium constant K in solution can be expressed as the reaction quotient,[14]

$$K = \frac{c_{D^{+}} \cdot c_{A^{-}}}{c_D \cdot c_A} \tag{2}$$

with the concentration c_i of the respective species, considering ideal behavior with activity coefficients of 1. Our measurements indicated that in the investigated systems there is always only 1 electron transferred, thus $c_{D^{+}} = c_{A^{-}}$ and $z_e = 1$. The solutions were mixed in a molar ratio of one acceptor per one donor molecule, therefore $c_D \approx c_A$. Since we assume no side reactions taking place, $c_A + c_{A^{-}} = c_A^0$, where c_A^0 is the starting concentration of acceptors in the mixed solution. Based on these considerations, we can estimate the percentage P of molecules, which undergo charge transfer $(P = c_{A^{-}}/c_A^0)$ in solution via

$$P = \frac{\sqrt{\exp\left(\frac{F\Delta E}{RT}\right)}}{\sqrt{\exp\left(\frac{F\Delta E}{RT}\right)} + 1} \ . \tag{3}$$

This formula shows the dependence of the charge transfer probability on temperature and the energetic difference in redox-potentials for a donor-acceptor system undergoing single charge transfer. It can also be easily modified to accommodate different molar mixing ratios of 1:r (dopant:host) and then reads

$$P = \frac{\sqrt{r \exp(\ldots)}}{\sqrt{r \exp(\ldots)} + 1} \ . \tag{4}$$

In cases of $E_{1/2}^{ox} \approx E_{1/2}^{red}$, where $\exp(\ldots) \approx 1$ and thus, the IPA yield for 1:1 ratios is only medium, P increases drastically for low dopant concentrations with $r \gg 1$. In such cases, low dopant concentrations of a few percent (as commonly used) have a higher ionization efficiency than molar mixing ratios of 1:1.

9. Scanning force microscopy of thin films

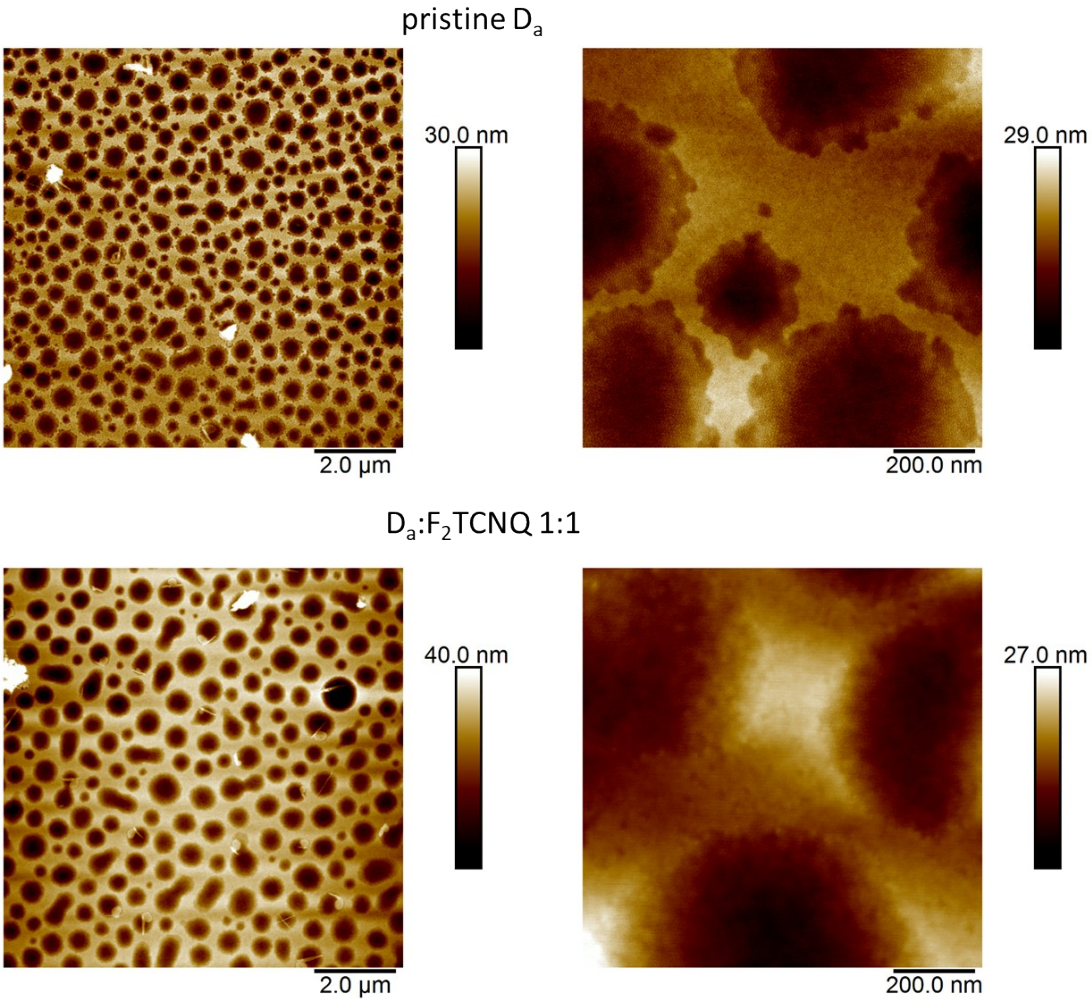

Figure S10. Representative scanning force microscopy images of thin films. Top row: pristine thin film of D_a. Bottom row: 1:1 molar ratio mixed film of D_a and F_2TCNQ. The very similar morphology suggests good mixing of the two molecules in thin films.

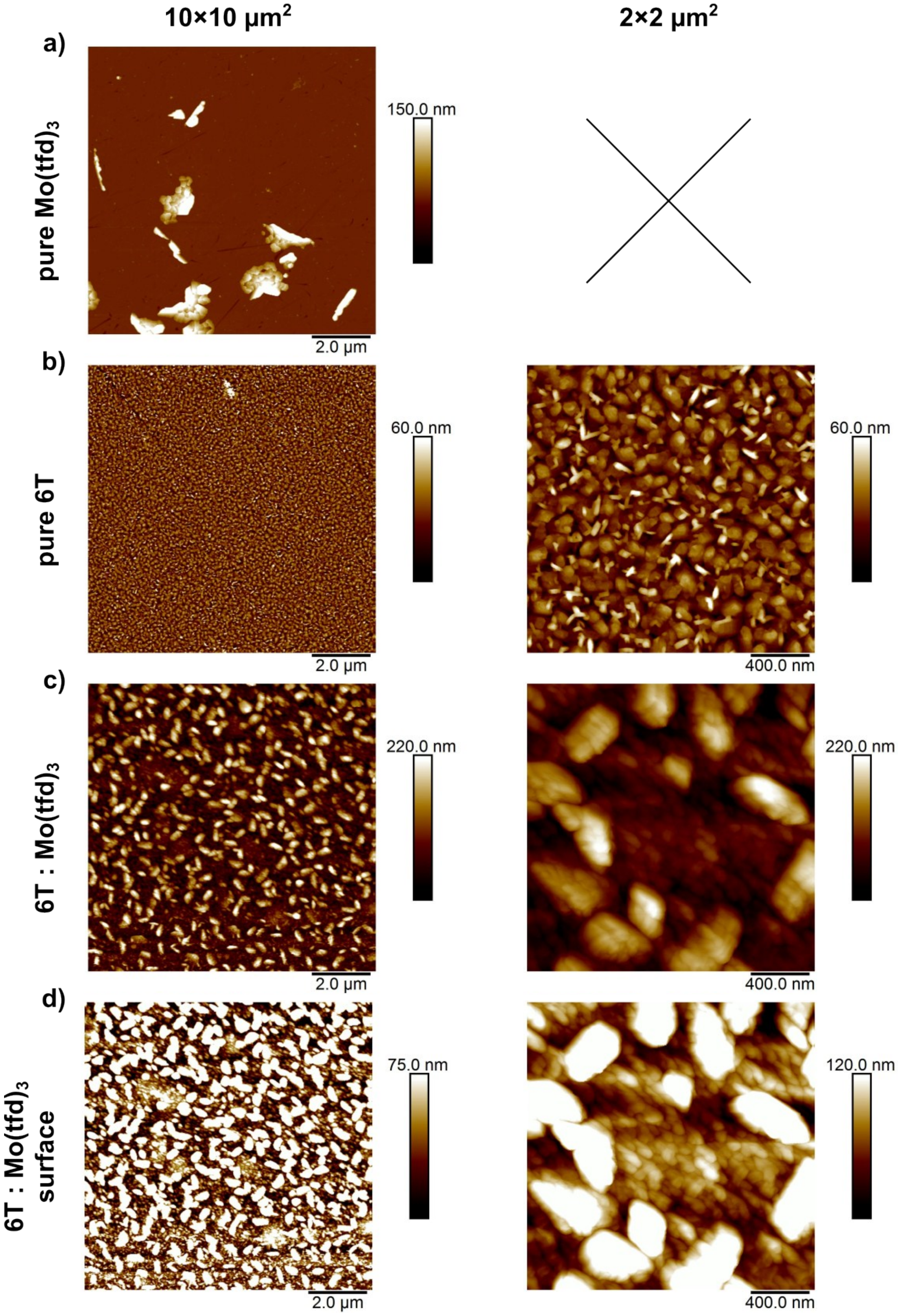

Figure S11. Scanning force microscopy images with size 10×10 µm^2 (left column) and 2×2 µm^2 (right column) of **a)** pure Mo(tfd)$_3$, **b)** pure 6T, **c)** mixed 6T:Mo(tfd)$_3$, and **d)** mixed 6T:Mo(tfd)$_3$ with a different height scale to enhance the area between protruding features. Pure Mo(tfd)$_3$ grows in large islands, while pure 6T grows in a homogeneous film with grains of diameter in the range of 150 nm. The mixed film shows a morphology with protruding high features, and smaller grains in between. This indicates that 6T and Mo(tfd)$_3$ do mix to some extent (inducing the much smaller grain size of low-lying features), but phase-separated islands of Mo(tfd)$_3$ may coexist.

10. References

(1) Chan, C. K.; Amy, F.; Zhang, Q.; Barlow, S.; Marder, S.; Kahn, A. *Chem. Phys. Lett.* **2006**, *431* (1–3), 67.

(2) Méndez, H.; Heimel, G.; Opitz, A.; Sauer, K.; Barkowski, P.; Oehzelt, M.; Soeda, J.; Okamoto, T.; Takeya, J.; Arlin, J.-B.; Balandier, J.-Y.; Geerts, Y.; Koch, N.; Salzmann, I. *Angew. Chemie Int. Ed.* **2013**, *52* (30), 7751.

(3) Fichou, D.; Horowitz, G.; Xu, B.; Garnier, F. *Synth. Met.* **1990**, *39* (2), 243.

(4) Qi, Y.; Sajoto, T.; Barlow, S.; Kim, E.-G.; Brédas, J.-L.; Marder, S. R.; Kahn, A. *J. Am. Chem. Soc.* **2009**, *131* (35), 12530.

(5) Facchetti, A.; Yoon, M.-H.; Stern, C. L.; Hutchison, G. R.; Ratner, M. A.; Marks, T. J. *J. Am. Chem. Soc.* **2004**, *126* (41), 13480.

(6) Fichou, D.; Nunzi, J.-M.; Charra, F.; Pfeffer, N. *Mol. Cryst. Liq. Cryst. Sci. Technol. Sect. A. Mol. Cryst. Liq. Cryst.* **1994**, *255* (1), 73.

(7) Wintgens, V.; Valat, P.; Garnier, F. *J. Phys. Chem.* **1994**, *98* (1), 228.

(8) Connelly, N. G.; Geiger, W. E. *Chem. Rev.* **1996**, *96* (2), 877.

(9) Bockman, T. M.; Chang, H. R.; Drickamer, H. G.; Kochi, J. K. *J. Phys. Chem.* **1990**, *94* (22), 8483.

(10) Klessinger, M.; Michl, J. *Excited states and photochemistry of organic molecules*; Wiley-VCH: New York, 1995.

(11) Sakamoto, Y.; Suzuki, T.; Kobayashi, M.; Gao, Y.; Fukai, Y.; Inoue, Y.; Sato, F.; Tokito, S. *J. Am. Chem. Soc.* **2004**, *126* (26), 8138.

(12) Zhang, F.; Kahn, A. *Adv. Funct. Mater.* **2018**, *28* (1), 1703780.

(13) Kanai, K.; Akaike, K.; Koyasu, K.; Sakai, K.; Nishi, T.; Kamizuru, Y.; Nishi, T.; Ouchi, Y.; Seki, K. *Appl. Phys. A* **2009**, *95* (1), 309.

(14) Atkins, P.; de Paula, J. *Atkins' Physical Chemistry*, 10th ed.; Oxford University Press: Oxford, 2014.